

# **Forest classification - Problem formulation and initial experiments**

Rune Solberg, Anne H. Schistad Solberg and Hans Koren

NR Note BILD/03/96

February 1996

## **Abstract**

The focus of the research presented in this report is the challenge of computer-based forest classification of digitized infrared aerial photography. Interpretation of such demanding imagery has until now exclusively been performed manually. The current research is a first step in the direction of the goal of semi-automatic interpretation of forest imagery. The first objective of the work presented has been to identify and define the problems of forest mapping in an as concise way as possible and in terms of a remote sensing approach. The second objective has been to do initial data exploration and tests of standard image analysis methods. It has been determined that the geometrical distortions in an aerial photography will heavily influence the performance of automatic classification if the effects are not modelled and corrected. The discrimination experiments show that both texture and spectral features to some extent may be used to discriminate tree species and cutting classes. In data with low geometrical distortion, some GLCM textural features showed good discrimination ability. Based on the distribution of a set of ten derived spectral classes, we can discriminate properly between: (i) spruce, cutting class 1; (ii) spruce and pine, cutting class 3; (iii) spruce, cutting classes 4-5; and (iv) deciduous forest.

# Contents

<b>1</b>	<b>Introduction</b>	<b>1</b>
1.1	Motivation . . . . .	1
1.2	Remote sensing in forestry today . . . . .	2
1.3	Which parameters to measure? . . . . .	3
1.4	Objectives . . . . .	3
<b>2</b>	<b>The test data set</b>	<b>5</b>
2.1	The test area . . . . .	5
2.2	Forest inventory reference data . . . . .	6
2.2.1	Mapped data . . . . .	6
2.2.2	Data quality . . . . .	7
2.2.3	Data selected for experiments . . . . .	8
2.2.4	Transformation of data . . . . .	11
2.3	Aerial imagery . . . . .	11
2.3.1	Infrared imagery . . . . .	11
2.3.2	Data set extracted . . . . .	12
<b>3</b>	<b>Imaging effects of forests</b>	<b>14</b>
3.1	Geometrical imaging effects in general . . . . .	14

3.2 Observed effects . . . . .	19
<b>4 Forest image features</b>	<b>21</b>
4.1 Spectral features . . . . .	21
4.2 The texture of forest . . . . .	24
<b>5 Initial data exploration</b>	<b>27</b>
5.1 Spectral experiments . . . . .	27
5.2 Textural experiments . . . . .	31
5.2.1 Description of method . . . . .	31
5.2.2 GLCM spectra experiments . . . . .	33
5.2.3 Forest-parameters-versus-texture experiments . . . . .	34
<b>6 Discussion and conclusions</b>	<b>41</b>

# Chapter 1

## Introduction

### 1.1 Motivation

The work presented here has been carried out in a project under the Norwegian Research Council's research programme *National Action Plan for Geographical Information Technology*. The project has been one of the Norwegian Computing Center's contributions to the methodological research carried out by SINTEF, Christian Michelsen Research (CMR) and Norwegian Computing Center (NR). Most of the research presented here has taken place in the period 1995 to early 1996. The work is followed up by further research in 1996 under the same programme and, hopefully, under new projects in the years coming.

The focus of the research presented in this report has been the challenge of forest classification based on digitized infrared aerial photos. Interpretation of such demanding imagery has until now exclusively been performed manually. The current research is a first step in the direction of the goal of semi-automatic interpretation of forest imagery. Operational semi-automatic mapping will probably be carried out on data originating from electrooptical and microwave sensors, however, this first steps of research have equally well been carried out on digitized infrared photos.

Operational semi-automatic classification of forest imagery will probably be a result of development on both classification methods and forest mapping practice. Remote sensing is about measuring physical and chemical properties of an object. However, forest mapping of today is more about classifying the forest into practical classes set by economic and managemental constraints. Forest mapping by remote sensing will definitely be much cheaper than the manual methods applied today, however, it is not possible to measure exactly all and the same parameters. The demand for more efficient forest mapping due to small economic margins will make an evolution towards a compromise between the level of detailed mapping and efficiency. Progressive forest managers say that this process may take 5-10 years.

Traditional satellite-borne remote sensing sensors has been determined not to be very suitable for forest mapping in heterogeneous forests, like the Norwegian forests (see e.g. (Strand 1989)). The spatial and spectral resolutions are too low, and not all important parts of the electromagnetic spectrum are covered. However, the fast technological development on remote sensing sensors will within a few years make the most fundamental information available to the Norwegian forest manager. The probably most important technologies are spectrometers, laser altimeters and multi frequency/full polarization synthetic aperture radars. This instruments are available with suitable configurations for airborne applications today, and they will be available in space around the change of the decade. It is expected that forest mapping will be much more efficient using such airborne sensors, and this may be the solution for about the rest of the decade. After this period, even larger savings will be obtained by using satellite-borne instruments that map larger areas for a lower price.

## 1.2 Remote sensing in forestry today

There is already a tradition for using remote sensing in forestry in areas with large and homogeneous forests. Canada has been in the forefront of using satellite imagery for this purpose. As an example, the Inventory Branch in the Ministry of Forests in British Columbia has the mandate to annually update the provincial forest inventory database which consists of over 6,600 1:20,000 scale map sheets (Pilon & Wiart 1990). Visual interpretation is here combined with computer assisted mapping (CAM) and a geographic informations system (GIS). Such a small revision cycle would not be possible with traditional aerial photography. This is illustrated by the fact that the revision cycle was 10 years in 1978.

There is a strong increase in the interest for application of remote sensing to determine forest health, both natural diseases and stress resulting from pollution. Spruce budworm damage has been studied by (Leckie, Yuan, Ostaff, Piene & MacLean 1992) in Canada. They studied whether MEIS (Multispectral Electro-optical Imaging Scanner) data could be used for identification of defoliation caused by the spruce budworm. They found good discrimination for levels of defoliation  $> 20\%$ , and concludes that high resolution MEIS data can be used for single tree defoliation assessments.

General stress of trees has been studied by Rock et al. (Rock, Vogelmann, Williams, Vogelmann & Hoshizaki 1986) with global forest health monitoring in mind as the ultimate goal. The main reason for the interest is that the growth rate and health of high-elevation spruce-fir forest in the north-eastern United States have declined markedly since the early 1960s. During the same period, a similar decline in spruce, fir, and beech has been documented in many parts of central Europe. The research group of Rock et al. at Jet Propulsion Laboratory (NASA/California Institute of Technology) has accomplished a programme to determine the effects of tree stress on the spectrum. They conclude that tree stress can be measured by remote sensing, and that broad-band sensors may suffice.

## 1.3 Which parameters to measure?

It must be assumed that remote sensing based forest mapping will not necessarily give the exactly same result as a manual mapping. (However, two manually made maps will almost always also be somewhat different!) A remote sensing system will use the measurements to determine classes based on physical/chemical properties alone. A forester may also take other, practical considerations into account when making a map.

A very fruitful dialogue has taken place between Glommen Skogeierforening and NR (catalysed by the GIS company TerraNor) with respect to forest mapping. This may be a first step away from thinking only in terms of "business as usual" to a creative process towards a solution of how to adapt traditional forest mapping to a more remote sensing-based forest mapping. The traditional way to do forest mapping has been to map all parameters each time. The advent of using GIS started a process to think about whether mapping could be done more efficiently by not ignoring the value of old information. There is a lot of information in a GIS, even if it is unrevised and ten years old!

Table 1.1 summarizes the dialogue. It shows the information required for a forest, in addition to a priority value showing the importance of the parameter. It also shows which parameters that change with time, and which parameters that can be regarded as constant. If a parameters is constant, much more resources can be applied to map it accurately once and for all (and there is not necessarily any need for remote sensing methods to measure the parameter).

Out of the 24 parameters, 8 may be considered constant and, therefore, should not be given strong attention for semi-automatic mapping. Some of the variable parameters may be derived from other parameters. *Tree volume* may possibly be derived from *crown diameter*. A better estimate may be derived from the combination *tree height* (measured by a laser scanner) and *crown diameter*. *Site index* may be derived from tree height and age. The parameter *age* is of no need to map, since it can be derived from already registered planting information.

## 1.4 Objectives

The first objective of the work presented in this report has been to identify and specify the problems of forest mapping in an as concise way as possible and in terms of a remote sensing approach. The second objective has been to do an initial data exploration and test of easily available image analysis methods. The findings from this early investigation represent a base to build on for selection of appropriate remote sensing sensors and develop suitable data analysis methods.

Parameter	Priority	Variable
Tree species	1	Yes
Stocking	2	Yes
Crown diameter	2	Yes
Volume	1	Yes
Height	1	Yes
Age	3	Yes
Health	1	Yes
Stand generation	1	Yes
Dry trees	1	Yes
Windfall	1	Yes
New clear cuttings	1	Yes
Site index	1	No
Groups of deciduous trees	1	Yes
Large single deciduous trees	2	Yes
Surface vegetation	1	Yes
Ground moisture	1	Yes
Soil depth	2	No
Soil texture	2	No
Ground surface structure	2	No
Terrain slope	2	No
Multi-layered	2	Yes
Scree	2	No
Landslide areas	2	No
Impediment	1	No

Table 1.1: *Forest parameters identified as important for forest mapping in Norway.*

# Chapter 2

## The test data set

### 2.1 The test area

The test area is located in Grue county, west of the river Glomma as shown in Figure 2.1. The rectangle shows the limits of the area covered by aerial images and the dashed circle shows the sub-area selected for extensive experiments.

The area is nearly completely covered with conifer forest, mostly spruce. There are some stands containing only pine, but in most cases pine grow together with spruce. Larger groups of deciduous trees are found only at the border of some of the marshes. Single trees and small groups of deciduous trees may be found spread among the spruce and pine. An extensive forestry has been effective for generations, and there are forest stands of all ages from 0 to 150 years.

A sub-area was selected for classification studies. This was done to reduce the amount of data and to reduce the influence of some of the imaging effects described in Chapter 3. The position of the sub-area is shown in Figure 2.1. It is a circular area of radius 1 km around the centre of an aerial image. As the distance from the centre of the image is less than 1 km, the radial effects will hopefully not be too disturbing. The main part of the area is fairly flat, however, there may be a few imaging problems due to some steep hillsides.

The sub-area was closely examined to see if it contained a representative collection of forest stands. It was found to contain a satisfactory distribution of different cutting classes and age classes. The area was chosen to get a relative high representation of pine stands. A part of the chosen area is covered by three aerial images.

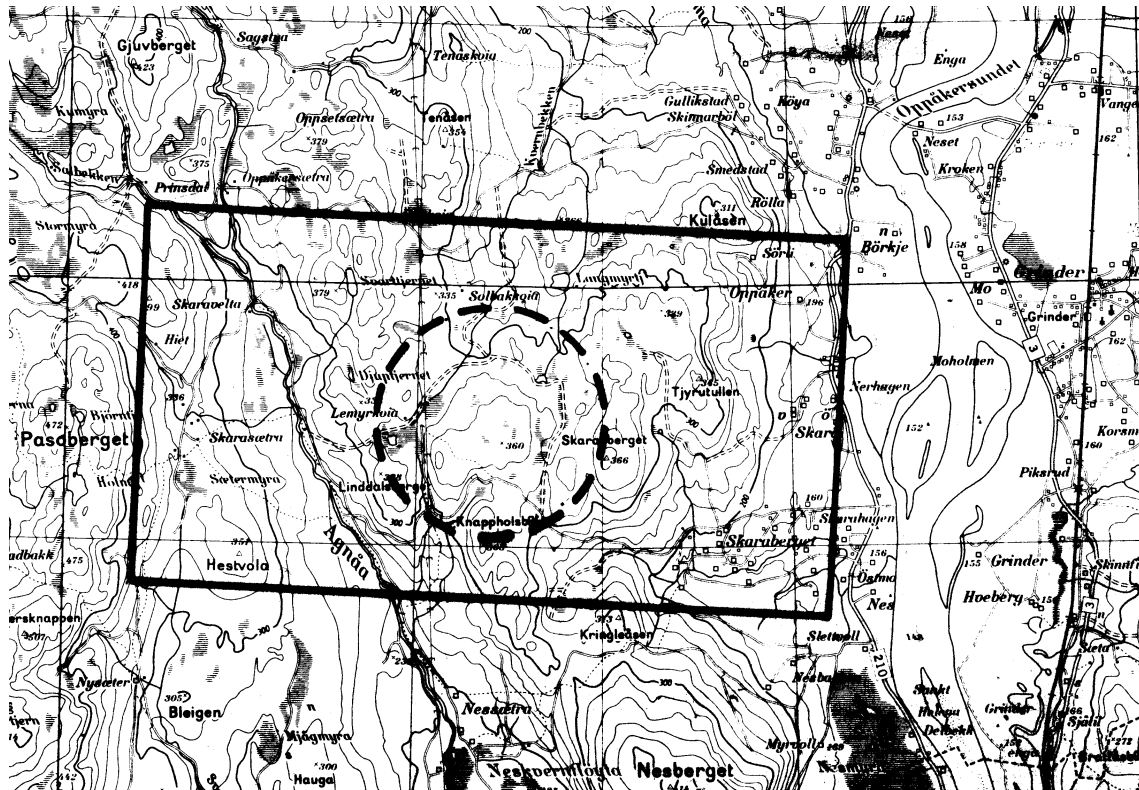


Figure 2.1: *Location of test area (scale 1:36,000). Dashed circle shows selected sub-area (adapted from M711 map, Norwegian Mapping Authority).*

## 2.2 Forest inventory reference data

### 2.2.1 Mapped data

A forestry map data base for the test area exists and map sheets have been derived from this. The data base was last revised in 1994. The forest is divided into *compartments* and *forest stands*. A forest stand is an aggregation of trees sufficiently uniform in composition to be distinguishable from adjacent areas. The grouping variables can be species composition, age classes, size classes, etc. Each compartment is identified by a number (e.g. 94006.1). In each compartment, the forest stands are identified by stand numbers counted from 1. The forest stands have been assigned different colours according to the cutting class in the stand. On larger scale maps (1:5,000), the site index and cutting class of the stand are printed on the map.

In addition to the described map data, the data base contains various data related to each forest stand. A set of about 100 different data types may be registered for each stand. The data refers to topographical and vegetational properties of the stand, properties of the trees in the stand, transport, planned activities, economy, etc.

It was easy to extract data relevant to the actual classification experiments from this

comprehensive data base.

## 2.2.2 Data quality

The data representing a stand are mean values. Measurements are performed at various sites throughout the stand, and suitable mean values are calculated. The classification is usually done by one person. The classification procedures may vary somewhat, and the same area may be classified differently by another person. Some details may be overlooked, and some may be considered insignificant. The result of the manual classification is a generalization. One has to be aware of this when comparing these data with an automatic classification.

When using the aerial images for automatic classification, details that have not been included in the manual classification data may occur. Some of these problems are mentioned below.

### Small diverging areas within a forest stand

To be registered as a forest stand, the area of the stand must be larger than some minimum value. Crops or unproductive areas smaller than this size will be included in a neighbour stand. Within a forest stand with a registered value of mean age and cutting class, there may be smaller areas with trees of another type, age or cutting class. The borders of these sub-crops are marked in the map, and should be considered when areas for training and classification are chosen.

In addition, there may be unproductive areas and aggregation of trees that are too small to be marked on the map. The contents of non-productive forest land (Norw.: impediment) within a forest stand is given by a number showing the percent of the area of the stand represented by non-productive forest land. The size of the non-productive forest land area will influence on the classification result.

Smaller crops or single trees different from the mean type in the stand may also create difficulties for the classification.

### Majority type of trees

Within a forest stand there may be trees of different types. This may complicate the classification procedure. The data base gives the “type of tree” (in Norw.: “bonitetstreslag”) of the stand. In our data set, this will be spruce or pine. But the data does not necessarily give you the main type of trees in the stand. For cutting class 2 and 3 and the lower age part of cutting class 4, it will give the majority type of tree, but for cutting class 5 and the

upper part of 4, it shows the tree type that would give the best production result in the area. And this is not always the actual majority tree type. This means that you have to find the majority tree type in another way.

## Distribution of tree types

In the data base, there are two sets of data giving a clue to the relative distribution of spruce, pine and deciduous trees within a stand.

For cutting class 2, the relative number of each type of tree has been estimated to the nearest 10% of the total number of trees. For cutting class 3, 4 and 5, the volume of each type of tree is given. From these numbers, the relative volume may be calculated to the nearest 10%.

It is difficult to tell the influence of these mixtures of tree types on the aerial image. The figures do not tell if the trees of one type are closely aggregated or spread throughout the whole stand. In these experiments, we have focused on stands having close to 100% of one type of trees.

### 2.2.3 Data selected for experiments

Data that are supposed to have an influence on the appearance of a forest stand in an aerial image have been extracted from the data base. The following data types have been extracted (all of them have not been used in the current experiments):

**Site index** This parameter tells something about the conditions for growth of trees in the area. For forest stands, the parameter may have one of the following values: 6, 8, 11, 14, 17, 20, 23. The higher the value, the better are the growth conditions. In addition, the parameter may tell if the area is of another type, not suited for growing timber. The following are examples of such area types:

- water
- marsh
- road
- non-productive forest land
- farm (or cultivated area)
- other type of area

**Cutting Class** This parameter divides the trees into five classes:

1. Newly cut site
2. Age 0 - 30 years, young trees, up to 6 - 7 meters high
3. Age 30 - 60 years, normal crown closure, younger productive forest
4. Age 60 - 90 years, older productive forest
5. Above 90 years, old forest

The cutting class does not follow the age precisely. The site index have a great influence too. In an area with a high site quality, the trees may be classified to a higher cutting class than the age should tell. In the test area, there are examples of trees of age 25 years and site index 17 that are classified into cutting class 3. In cutting class 4, you may find trees of age 40 and site index 20 and trees with age 95 and site index 11. In cutting class 5, you may find trees of site index 20 down to 70 years of age. Examples of the relations between age and cutting class for spruce in the test area are found in figure 2.2.

**Density** The density of the forest is registered in two classes: normal and thin. Most of the forest in the test areas has normal density. In a forest with scattered population of trees (thin) you may see much more of the ground between the trees. This will certainly have influence on the classification.

**Age class** The mean age of the trees in a stand is registered in steps of five years. The look of the trees from above will gradually change with age. However, the site quality have a great influence. Trees in a site with high quality will look older than the trees of the same age in a site with bad quality.

**Tree type** This value should tell you the main type of trees in the stand, but does not always so (see Section 2.2.2). It has not been used in this experiment.

**Number of trees** For cutting class 2, the relative number of spruce, pine and deciduous trees are given to the nearest 10%.

**Volume of trees** The separate volumes of spruce, pine and deciduous trees within the stand are registered. For cutting class 3, 4, and 5, the relative volumes are calculated to the nearest 10%.

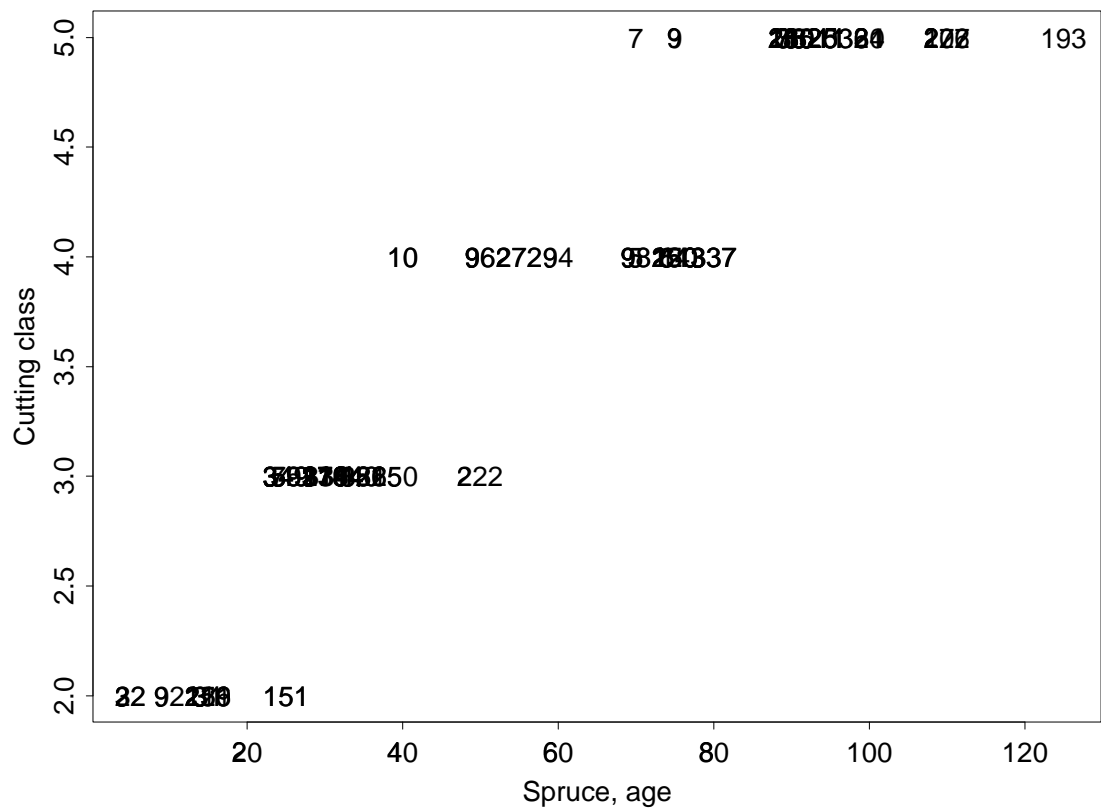


Figure 2.2: *Cutting class as a function of age for stands with 100% spruce (the numbers are stand numbers).*

**Non-productive forest land** The area of non-productive forest land in the stand is registered in percent of the total area. When non-productive forest land is present, there will be areas without trees in the stand.

## 2.2.4 Transformation of data

From the digital, vector-based forestry map data, a set of raster masks have been constructed. Arc/Info was used for this purpose. Each mask covers the sub-area chosen for experiments. The pixels within a forest stand are assigned a pixel value (code) corresponding to the value of one special parameter. Masks have been created for the following parameters:

- Forest stand no.
- Cutting class
- Forest density
- Age class
- Site index
- Relative amount of spruce
- Relative amount of pine
- Relative amount of deciduous trees

The masks were first created in the actual map projection. Then, the coordinates of a set of corresponding points were found on the mask and the scanned image. Using these coordinates (control points), a geometric transformation was performed to make the masks match the image geometry. Combining the image with the forest stand mask makes it easy to find the forest stands in the image. The cutting class mask identifies all areas with a certain cutting class, and so on.

## 2.3 Aerial imagery

### 2.3.1 Infrared imagery

The image data applied in the experiments is derived from aerial photographic film. The photos were taken by Fotonor A/S (job no. 94169) on August 16, 1994 at about 11 AM flying in a direction approximately west to east. The exposures were taken with a Leica

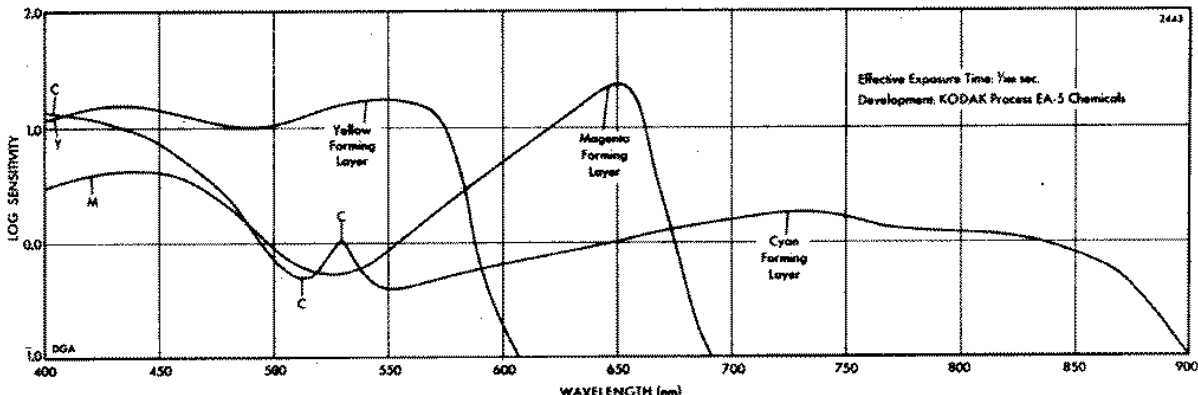


Figure 2.3: *The sensitivity curves for the three emulsion layers of the Kodak Aerochrome Infrared Film Type 2443 (courtesy Kodak Inc.).*

30/4 camera equipped with a lens of 55 degrees aperture angle. A Partenavia P68TC0 aircraft was used. The approximate flying altitude was 700 m above the terrain (950 m a.s.l). The photographic film used was Kodak Aerochrome Infrared Film Type 2443. It has a standard format of 23 cm × 23 cm. Wavelengths shorter than 525 nm are removed by a Kodak Wratten Filter No. 12. This positive colour film is rated to the Effective Aerial Film Speed (EAFS) 40. The film has been developed by a negative process producing a positive transparency.

The sensitivity curves of the three emulsion layers are shown in Figure 2.3. The approximate effect of the film is to register electromagnetic radiation in the three bands 525-580 (green), 580-680 (red) and 680-900 nm (infrared). For comparison, the corresponding bands for the SPOT HRV sensor are 500-590, 610-680 and 790-890 nm. As can be seen from the sensitivity curves, the film is much more sensitive in the two visual bands than the infrared band. The reason is that the film is made for vegetation mapping, and vegetation has very large reflectance in the near infrared. The visual result is a balanced contribution to the colours.

The film was digitized using a Intergraph PS 1 scanner. The scanning process was accomplished in three iterations using a red, green and blue filter, correspondingly.

### 2.3.2 Data set extracted

The location of the images is shown in Figure 2.1. The area is covered by three aerial images, numbered B6, B7 and B8 from west to east, with 60% overlap.

The images have been scanned by Fotonor AS with a resolution of 30 micrometers per pixel. The photographic scale is approximately 1:15,000. This gives a resolution of approximately 0.45 m per pixel in the terrain. The scanned data was delivered in three colour bands, in total nine single band images of size 7,680 × 7,680 pixels.

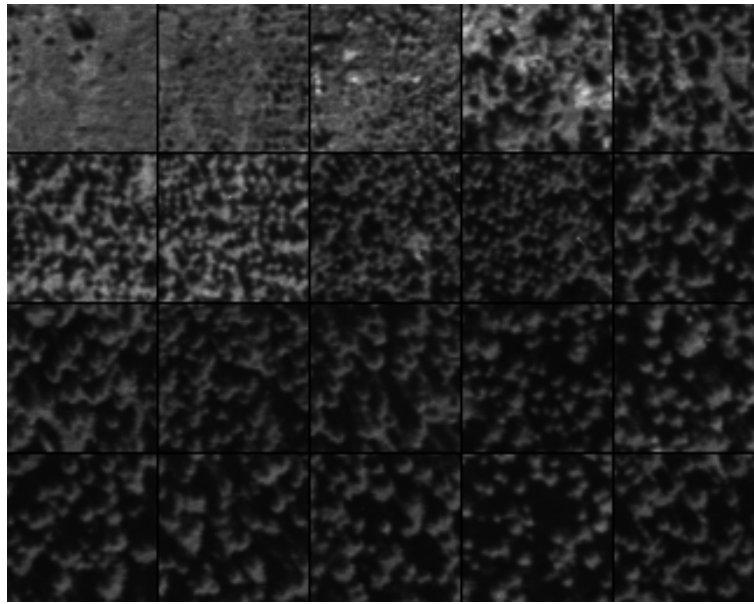


Figure 2.4: *Examples of forest stands. Each row represents one cutting class, with class 2 at the top and class 5 at the bottom.*

Before we got the digital site data, a preliminary set of test data was selected from the images using the paper version of the forestry map. A number of sub-images were created by selecting representative areas from sites with different qualities. The positions of the sub-images were determined by comparing the map with the aerial photographs visually. A size of only  $64 \times 64$  pixels was chosen to be sure that the whole sub-image was located within the actual forest stand. The locations were chosen as to avoid deciduous trees within the sub-images. Deciduous trees can easily be spotted by their colour in the aerial photographs. The sub-images were extracted from the blue band (covering an interval about “green” in the electromagnetic spectrum) in all the three images.

Examples of these sub-images are found in Figure 2.4. The examples are taken from stands with 100% spruce (exceptions for two examples of cutting class 2), located near nadir. The stands are ordered according to age (from 5 to 125 years) and cutting class (2, 3, 4 and 5). Data for the stands, stand number and age are shown in Table 2.1.

32	117	216	63	41
5	10	15	20	25
349	331	276	186	222
25	30	30	35	50
94	98	61	220	337
60	70	75	75	80
130	64	202	126	193
90	100	110	110	125

Table 2.1: *Forest stand no. and age for the stands in the previous figure. All stands have 100% spruce, except stand no. 63 and 41.*

# Chapter 3

## Imaging effects of forests

### 3.1 Geometrical imaging effects in general

Ideally, at least from the viewpoint of digital image processing, the image forming geometry should correspond to a normal projection (see e.g. (Solberg 1985)). Geometrical imaging effects would then be position independent in the image. However, this is not obtainable in practice. An aerial camera will form the image by a process that corresponds approximately to a central projection. In comparison, a scanner or pushbroom sensor will form an image by a process corresponding to a central projection in the cross-track direction and a normal projection in the along-track direction.

An image cannot physically be formed by a central projection, and there will be various errors resulting in slight deviations from a central projection geometry. First, the optical system is not perfect. The optical elements are manufactured in a process giving a rotation-symmetric result. Hence, the error is only depending on the radial distance from the optical axis. The resulting errors represent radial displacements towards (-) or away (+) from the optical axis. Figure 3.1 shows a typical error curve for an aerial camera. The maximum error is typically  $\pm 3\mu\text{m}$ . Compared to the scanning resolution of  $30\ \mu\text{m}$  used in the current experiments, the error is of no significance here.

Another main error source is refraction. Figure 3.2 shows, very exaggerated, the path of a light ray inclined to the optical axis. As we can see from the figure, the resulting effect is a radial displacement away from the optical axis. Figure 3.3 shows error curves as function of the distance from the optical axis for various flying altitudes. The altitude was approximately 950 m a.s.l. for the image applied in the current experiments, giving a maximum error of about  $+3,5\ \mu\text{m}$ . This error is also neglectable taking into account the scanning resolution.

A flat surface oriented parallel to the film plane will be imaged in a conform way. The situation changes when the ground surface and the image plane is not parallel. A point

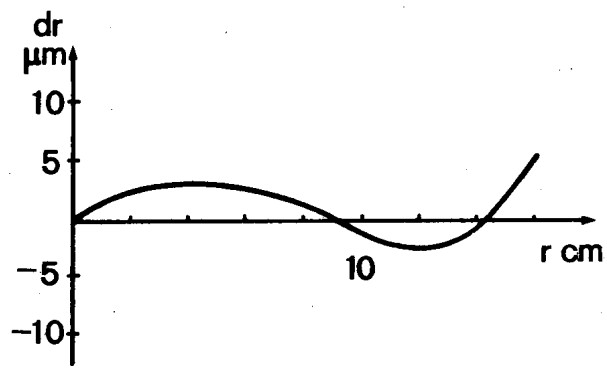


Figure 3.1: *The radial displacement error curve of a typical aerial camera lens (from Nämnden för Skoglig Fjärranalys, 1993).*

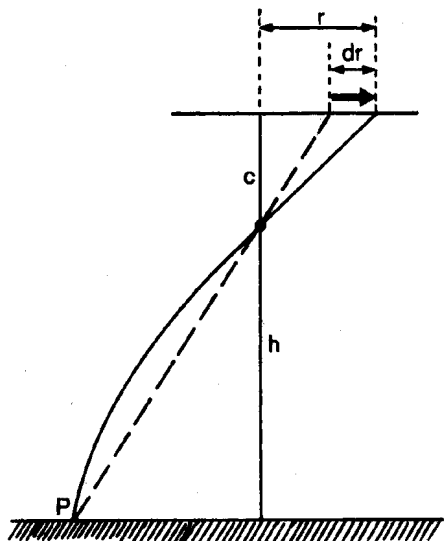


Figure 3.2: *Atmospheric refraction generates a radial displacement away from the optical axis (from Nämnden för Skoglig Fjärranalys, 1993).*

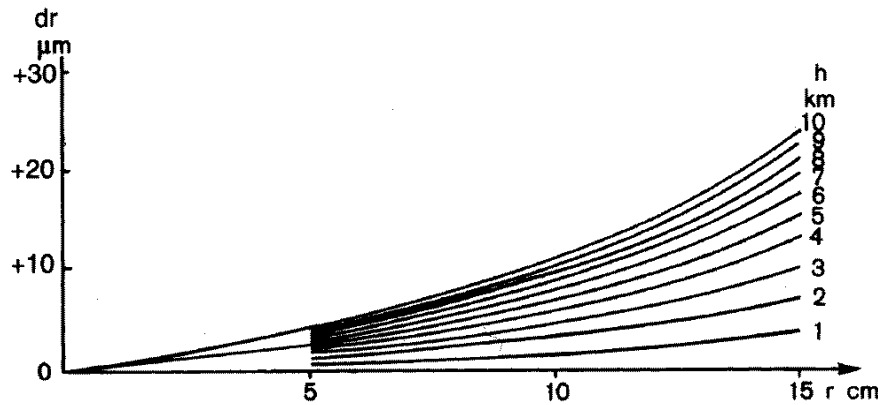


Figure 3.3: *The atmospheric refraction as a function of the distance from the optical axis given for various flying altitudes. The refraction increases with altitude since the light has to pass several atmospheric "layers" of different refraction index (from Nämnden för Skoglig Fjärranalys, 1993).*

nearer the camera than the parallel surface is imaged further from the optical axis than a corresponding point on the surface. Correspondingly, a point further away will be imaged nearer the optical axis. The height-dependent effect is like the other effects a radial displacement. The displacement  $dr$  (AB in Figure 3.4) is given by

$$dr = h \tan \theta \quad (3.1)$$

where  $h$  is the elevation deviation and  $\theta$  is the observation angle (measured from the nadir point). The effect is important when interpreting imagery where  $\theta$  is not very small, as for aerial imagery. (The effect is small for narrow-angle satellite sensors, see (Solberg 1985).) In forestry mapping, radial displacements originating from tree heights and terrain elevation variations must be taken into account. The terrain elevation variations will result in positional errors if one cannot compensate for the true elevation. The tree height results in a radial distortion effect when a tree is projected onto the film plane. As can be seen from Equation 3.1, the effect is most prominent far away from the nadir point. Figure 3.5 illustrates the effect for cone-formed objects (spruce trees).

The combined effects of the solar illumination direction and the radial distortion of the trees create a very characteristic tree pattern in a forest. However, the pattern depends on the position in the image, and this makes automatic tree classification a more complex task, both from a spectral and a textural viewpoint. Figure 3.5 illustrates these effects. The pattern can be divided into three type of segments: sunlit tree segments, self-shadow tree segments (the dark side of a tree) and tree shadows. A fourth could also be included, the ground surface, depending on the tree density. The figure shows the situation at noon, when the sun is culminating in the south direction. The northern side of the image is dominated by sunlit trees with a small fraction of tree shadows. The sunlit fraction decreases towards the south in the image, and the self-shadow segment is totally dominating in the southern part. The area of tree shadows is increasing towards nadir since each tree and its neighbours

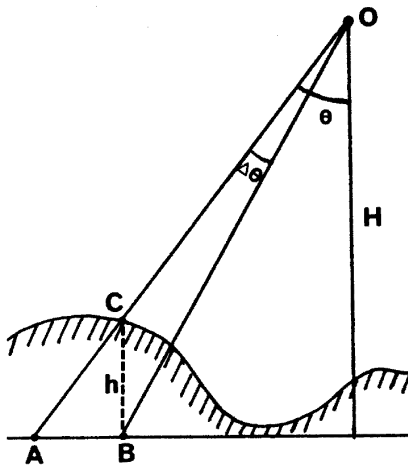


Figure 3.4: *The radial displacement due to deviations from a flat surface parallel to the film plane. A point C on the terrain surface will be expected to be located at A if the surface were flat. However, the correct location should be B (from Solberg 1985).*

are obscuring less of its own shadow. The variations are most extreme along the central north-south axis of the image, and least toward the western and eastern sides. More of a tree's shadow is visible towards the sides in the northern image part, and there is still a significant sunlit part towards west and east in the southern part.

For spectral classification, one has to take into account the three (four) types of segments. This could be done by assigning the components to two classes, *sunlit trees* and *shadows* (and possibly ground surface). When applying measures of texture, one must take into account that the textural variations within a homogeneous monoculture of trees due to the imaging effects may be larger than the variations between the various species (where spruce and pine are most important). One way to solve this problem is to model the imaging effects, i.e. the illumination and radial displacement. A special textural measure could be made with such a model built into it.

Terrain slopes will exaggerate the combined illumination and radial effects. Figure 3.6 shows the effect in the nadir situation. On the slope away from the sun, each tree will cast a larger shadow on the neighbour tree. The result is that only tree tops map be sunlit. The opposite is the case for a slope towards the sun; the sunlit area will increase.

As with the combined illumination and radial effects, this effect may be modelled. This requires a digital terrain model of very high resolution. The standard  $100 \times 100$  m grid from the Norwegian Mapping Authority will clearly not suffice. However, a very accurate model could be generated by using a laser range scanner (lidar). Such instruments are available and could be used in combination with standard aerial photography.

(For more about imaging effects, see e.g. (Nämnden för Skoglig Fjärranalys 1993) and (Howard 1991).)

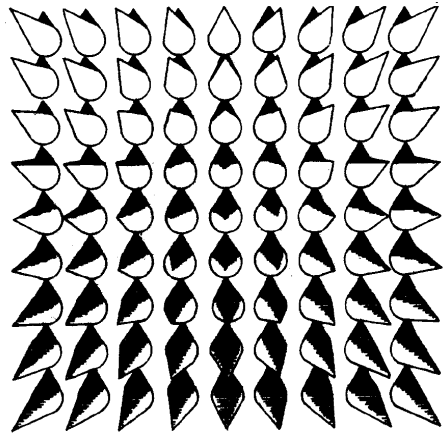


Figure 3.5: *The combined effect of radial displacement due to the vertical extent of a tree and the solar illumination creates a very characteristic pattern in a forest (from Nämnden för Skoglig Fjärranalys, 1993).*

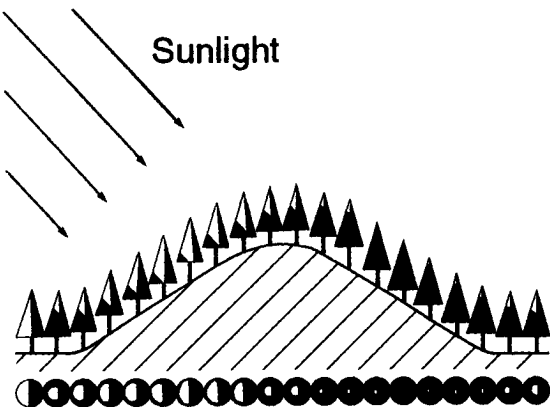


Figure 3.6: *Terrain slopes creates variations in the textural pattern created by trees in a forest. The trees are shown as seen from above in the lower part of the figure. (from Nämnden för Skoglig Fjärranalys, 1993)*

## 3.2 Observed effects

An example of radial distortion of trees in our data set due to the radial displacement's dependence on local height is shown in Figure 3.7. A sub-image of the same part of a stand of cutting class 5 is taken from two different aerial images. To the left, the stand is located about 350 meters from nadir. To the right, the same stand has a distance of 1,550 meters from nadir. The sunlight is coming from the lower right in both cases.

Here, the radial distortion effect is clearly demonstrated. We can see how the shape of each tree has been elongated, and the light intensity has been reduced as the distance to nadir has increased. The reason for the latter effect is that more shadows are observed per area unit in the right image than in the left.

The combined effects of varying distance to the nadir and the illumination direction are shown in Figure 3.8. Here, a set of sub-images of forest stands of cutting class 5 with different distances and directions relative to the nadir point is shown.

The centre sample is located close to the nadir (about 150 m). The samples on the diagonal from upper left to lower right are located close to the direction of the sunlight. The direction towards the sun is to the lower right. The samples on the other diagonal are, hence, located close to a line perpendicular to the direction of the sunlight. The distances from nadir varies from 1,000 m to 1,550 m for the outer four samples and from 350 m to 600 m for the inner four.

The effect of the sun is clearly seen on the samples along the diagonal towards the sun. As we move away from the sun, we see that each tree gets more of the sunlit side towards the camera. The area of bright parts increases and the shadowed area decreases. In the direction towards the sun, only the outlines of the trees are seen with sunlight, and the shadowed areas will increase.

In Figure 3.9, an example of the combined effect of sun and terrain is demonstrated. The figure shows two examples of forest stands of cutting class 4. The left stand is located in flat terrain. The right sample is located on a slope leaning away from the sun. Here, the trees will cast more shadows on their neighbours and the shadowed areas will increase. The

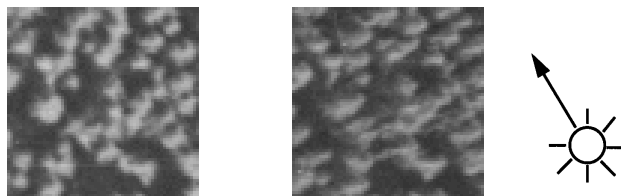


Figure 3.7: *Radial effect. The same forest stand (spruce, cutting class 4) photographed with a distance of 350 meters (left image) and 1,550 meters from nadir. Nadir is located to the left of the stands. The direction of the sunlight is shown to the right.*

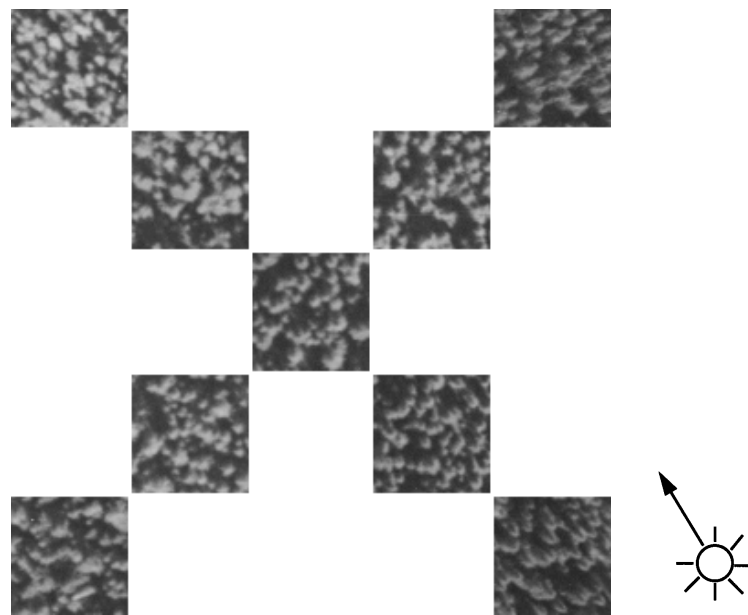


Figure 3.8: *Effects of the solar illumination direction.* Forest stands located along the direction of sunlight and perpendicular to this direction are shown. The centre image is near nadir. The sunlight is coming from the lower right.

steeper the hillside, the smaller part of each tree will get into the sunlight and the larger the shadowed area will be.

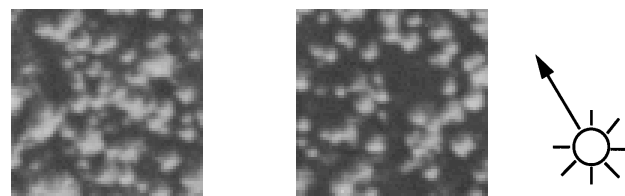


Figure 3.9: *Combined effect of sun and terrain.* To the left, a forest stand of cutting class 5 is located on flat terrain. To the right is the same type of forest stand on a hillside with the slope pointing away from the sun. Nadir is located slightly up to the right. The distances from nadir to the stands are 650 m and 450 m, respectively. The direction of the sunlight is shown to the right.

# Chapter 4

## Forest image features

### 4.1 Spectral features

Vegetation is characterized by high reflectance (from mesophyll) in the visible and near-infrared part of the electromagnetic spectrum. There is a steep fall in the reflectance from the infrared towards the visible region due to high pigment absorption (from chlorophyll and caroten) (Figure 4.1). In addition, there is a sun-induced fluorescence in a narrow part of the spectrum (at about 685 nm). By observing features of the spectrum of vegetation, one has determined connections between these features and biochemical and physical properties, like water content, cellulose, and nitrogen and lignin in the foliage ((Tucker 1976), (Rock 1982)).

Research has determined relationships between characteristics in the spectrum of vegetation and stress factors, like air pollution, minerals/chemicals and drying ((Tapper & Dempsey Houston, Texas, May 16-19, 1988), (Singhroy, Stanton-Gray & Springer Reno, Nevada, Sept. 29 - Oct. 2, 1986), (Rock, Hoshizaki & Miller 1988), (Herrmann, Rock, Ammer & Paley 1988)). Stress factors change the absorption maximum of chlorophyll and the steep fall about 700 nm (Figure 4.2). In addition, the degree of absorption from tannin and anthocyanin is an indication of stress at an early stage.

Spectral properties of vegetation can be used to discriminate various species. Figure 4.1 shows the spectrum of four vegetation species. Note the large differences between the species for wavelengths longer than about 750 nm. Therefore, the infrared part of the spectrum is particularly suitable for vegetation discrimination. The spectra shown in Figure 4.1 are somewhat idealistic. Each curve must be interpreted as a mean value curve, and there may be considerable variations around this. Note also that pine in general has higher reflectance than spruce (fir). This is partially due to a shadowing effect. The sprigs of pine are generally less dense than of spruce, and the net effect is a brighter appearance of pine.

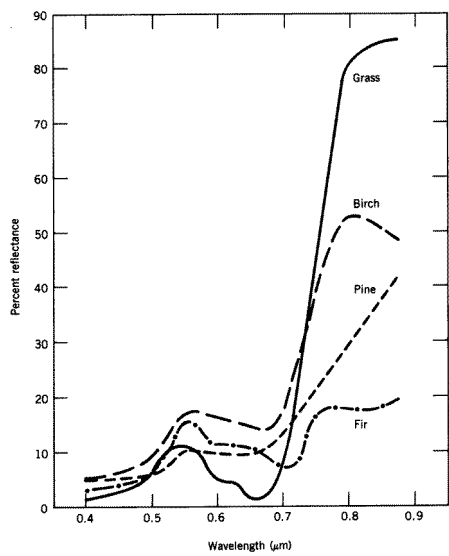


Figure 4.1: *Typical reflectance spectra for some vegetation types (from Elachi 1987).*

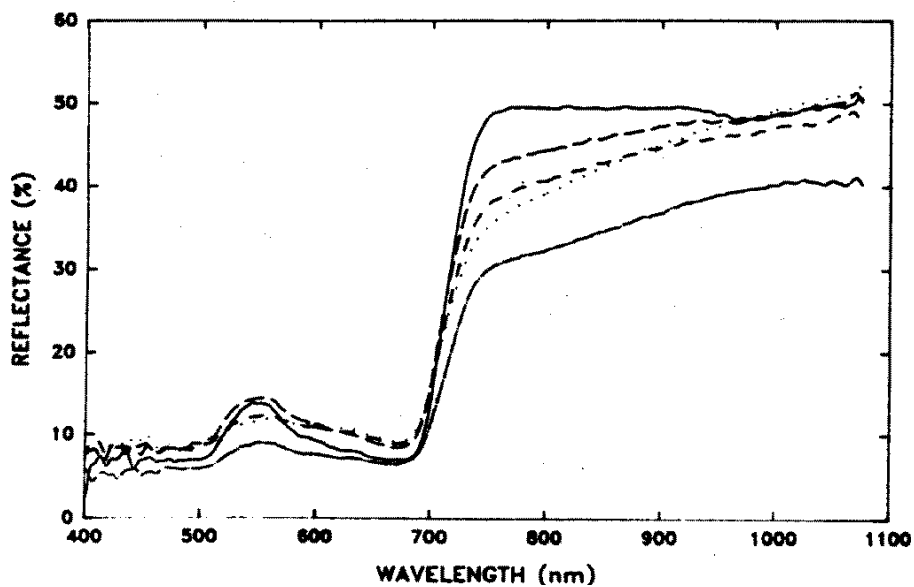


Figure 4.2: *Different degrees of fungus disease on deciduous trees, from 0% infection (upper curve) to 85% infection (lower curve).*

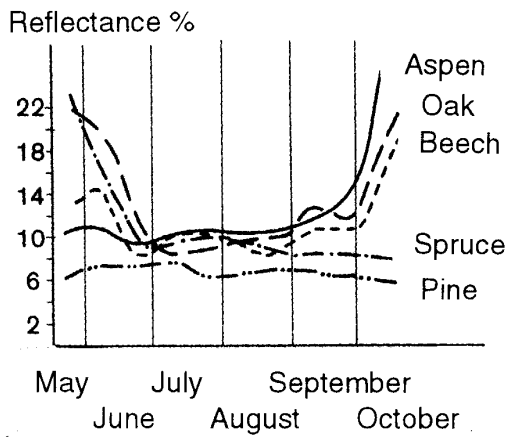


Figure 4.3: *Typical temporal changes of some conifer and deciduous species (adapted from Nämnden för Skoglig Fjärranalys, 1993).*

Spruce and pine do not have very dissimilar reflectance curves, and can under various conditions be difficult to discriminate. However, there are seasonal variations, and these may be used to obtain maximum discrimination. In particular, spruce has especially high reflectance in the early summer due to annual shoots and flowering (Figure 4.3). Similarly, dense appearance of cones will rise the reflectance curve in the late summer. However, initially spruce is darker than pine so these temporal effects may also make the reflectance more similar depending on the density of annual shoots, flowering and cones. In general, the best time for discrimination of spruce and pine is when the annual shoots are well developed for spruce, but before they are developed for pine.

The deciduous trees have highest reflectance in the infrared shortly after leafing. The reflectance is continuously decreasing towards the mid summer. Since the reflectance at the same time may increase for spruce due to annual shoots, the reflectance will be more similar towards mid summer.

A young spruce tree will have high reflectance in the infrared and low in the visible. This will change with the age of the tree. An old tree will have increased reflectance in the visible and decreased reflectance in the infrared.

It follows from this brief description of the electromagnetical properties of vegetation that the infrared part of the spectrum gives a lot of information about the type and state of the vegetation. This is also the motivation for the application of infrared film in forestry. Even if the dynamic area of visible black and white film is much larger than for infrared film, infrared film is usually preferred due to all the information gathered in the near-infrared and visible simultaneously (see Section 2.3.1 for more on infrared film).

Most satellite and airborne electro-optical sensors are designed with vegetation mapping in mind. Therefore, they usually cover the infrared as well as the visual part of the spectrum. Figure 4.4 shows the coverage of some important sensors. Note that the radiance is measured in broad bands, quite like infrared film. A comparison of the width of these bands with the spectral characteristics of each species or variations in the state of the

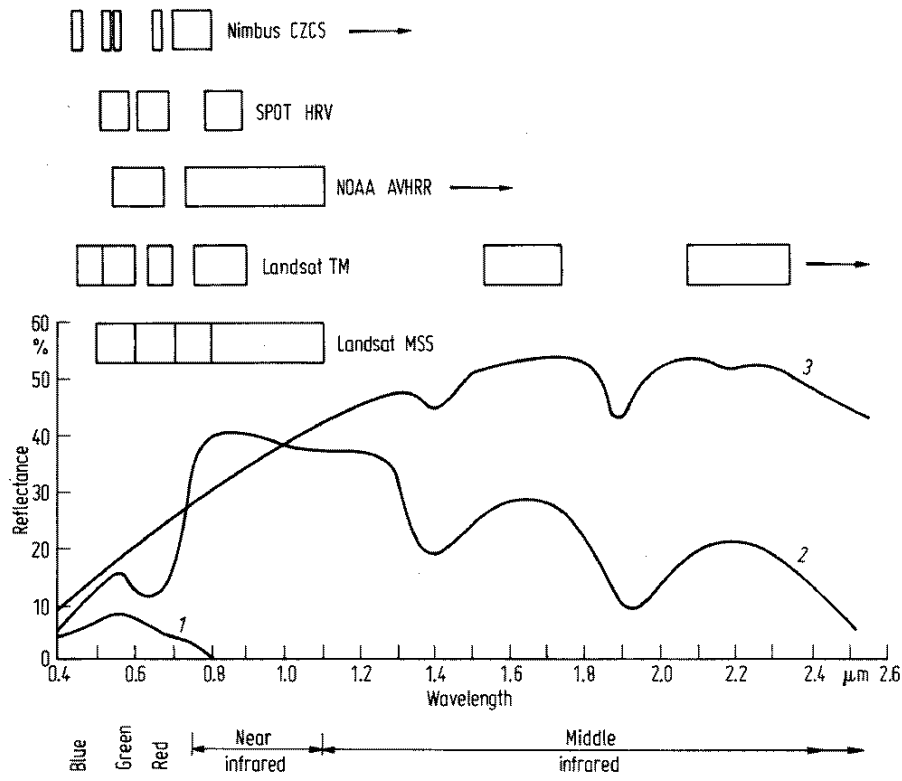


Figure 4.4: *The coverage and approximate bandwidth of the most important broad-band satellite sensors the last ten years (from Richards 1986).*

vegetation (e.g. due to stress), shows clearly that the spectral differences or variations have to be large to be measurable. Therefore, we must expect less good results with respect to discrimination and health measurements as long as we have to use broad-band electromagnetic sensors or infrared film as data source.

Imaging spectrometers, the new generation of electro-optical sensors, will to a large degree solve this problem by measuring the radiance in a long series of very narrow bands. However, the mixture of a lot of spectra will pose a large problem if the forest is very heterogeneous. This problem can be limited by using an optimal spatial resolution so that each pixel in general will cover one or two species only.

## 4.2 The texture of forest

Similarly to colour, the texture of a forest is an important feature for the photo interpreter in discriminating between various tree species. Hence, texture should be an important feature for automatic discrimination also.

Figure 4.5 shows the typical shapes of four common tree species (adult trees). Spruce has a typical cone-like shape and very dense sprigs. Therefore, the shadow has a cone-like shape

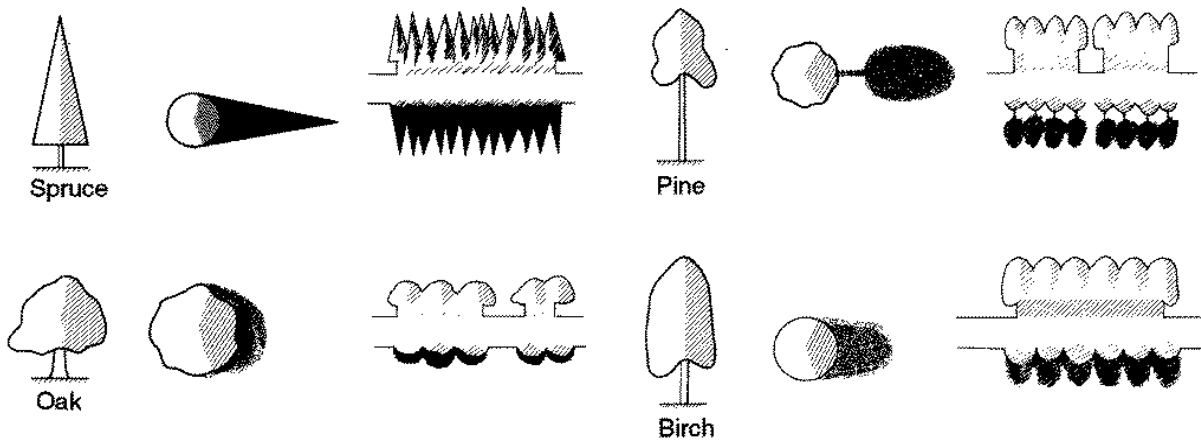


Figure 4.5: *Typical shapes of adult trees of four species. Shadow shape and darkness is also indicated (adapted from Nämnden för Skoglig Fjärranalys, 1993).*

and is very sharp. Most of the sprigs of pine is located in the upper half of the tree and has a dome-like shape. The shape is more irregular than for spruce, and the sprigs are less dense. The shadow is more elliptical and less sharp. Oak has a very wide crown, but the shadow is not so sharp as for conifer trees. The width of the birch crown is similar to pine, however, not so sharp. The shadow is also connected to the tree since most of the trunk is covered by branches.

Young spruce and pine trees are very similar in shape. However, the density of the sprigs of spruce is larger than for pine. The result is a smoother texture for pine.

In a textural context, the tree shapes, their shadows and shadow contrast, may be regarded as features of textural elements. If the stand is sufficient homogeneous, the texture may be characteristic for the species in the stand.

When using a textural measure as a feature in classification, it is important to take care of the variations generated from imaging effects due to radial displacement and illumination, as described in Section 3.1. The species' characteristic texture described here will in large parts of an aerial image be marginal compared to the imaging effects. Therefore, good textural discrimination may not be expected before the textural measurement method also models and compensates for the imaging effects.

The visual impression of the stand in an aerial image will change with the variation in some of the forestry parameters. The following parameters will have an influence on the texture (only conifer is discussed):

**Type of tree.** There is some difference in shape between spruce and pine, depending of the age, as described above.

**Age.** The size and shape of the crown changes with age. The difference is very little for young trees, but will increase with age.

**Site index.** The site index has an influence on the growth of the trees. Two forest stands with same age but different site index may look different.

**Cutting class.** This parameter is a function of *age* and *site index*. It will reflect the size of the trees. Forest stands within the same cutting class, will probably have quite similar texture.

**Density.** The density of the forest will have a large influence on the texture.

**Position.** The position of the forest stand will have an influence on the texture in more than one way. The topographic position will determine the *site index*, mentioned above. In addition, the position will have an influence on the texture due to imaging effects (see Section 3.1). This means that the texture of a specific forest stand may change between aerial images, according to the location of nadir and date and time of the recording.

# Chapter 5

## Initial data exploration

The purpose of the work presented here has not been to do a thorough data exploration, but to establish an initial feeling for the appropriate direction for further data analysis. The experiments cover analysis of both textural and spectral features.

To properly classify a forest scene, both spectral and spatial information must be utilized. Additional information in the form of map data from previous surveys should also be used. Spectral information is available in the three multispectral bands of the original image. Spatial information is computed in terms of texture modelling.

### 5.1 Spectral experiments

The original aerial image consisted of three spectral bands in the green, red, and near infrared part of the spectrum. Based on visual inspection of the aerial images, we have defined a set of nine “natural” classes which we expect the spectral information might be able to discriminate. The following classes are used:

1. Shadow
2. Soil (clear-cut areas and vegetation-free areas)
3. Shrub
4. Dry grassland (very sparse green vegetation)
5. Deciduous forest
6. Impediment (mostly rock, often covered with lichen)
7. Peat

Class centers, band 1 and 3

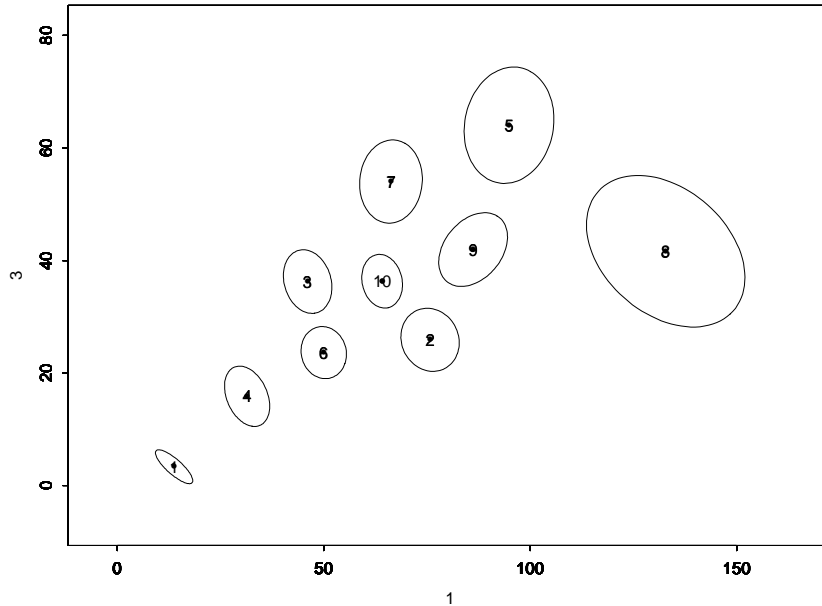


Figure 5.1: *The spectral classes visualized in the 2-dimensional feature space spanned by the spectral bands 1 and 3 (green and near infrared).*

- 8. Areas which are over-exposed during imaging (close to saturation)
- 9. Conifer, young
- 10. Conifer, older

From each of these classes, a few sample pixels are identified manually. These samples are then used as input to a clustering algorithm. Cluster analysis organizes the data by abstracting underlying structure by grouping individual image pixels. Cluster analysis is called unsupervised learning because it does not require any assumptions about the particular distribution of the data. The K-means clustering algorithm is used here (Jain & Dubes 1988). The clustering refines the cluster means in an iterative process.

After clustering, an initial segmentation of the scene into the classes listed above results. This segmentation is used to train a supervised Gaussian classifier. For each class, the mean and covariance matrix is estimated.

The resulting class centers can be visualized in the feature space (Figure 5.1). The class centers are given by the centers of the ellipses. The ellipses show the variance within each class; data within one standard deviation from the class mean will fall within this ellipse. The classes are very well separated. This could be expected given that their seed values were defined as the set of natural classes we would expect to discriminate given the spectral bands in the input image.

The next step in the data analysis is to relate the spectral classes to the desired cutting classes and tree types. In our test image, the following cutting classes are present:

- Spruce, cutting class 2 (S2)
- Spruce, cutting class 3 (S3)
- Spruce, cutting class 4 (S4)
- Spruce, cutting class 5 (S5)
- Pine, cutting class 3, young (P3Y)
- Pine, cutting class 3, older (P3O)
- Pine, cutting class 4 (P4)
- Deciduous forest

Pine, cutting class 3 has been divided into two subclasses based on manual inspection of the original image.

Figure 5.2 shows histograms of the distribution of the ten spectral classes for each cutting class and tree type. For each histogram, the *x* axis shows the spectral classes and the *y* axis their relative frequencies. To produce the plot for a given cutting class, the distributions of each spectral class was computed for all the forest stands of the given class in the test image.

We see that the distribution for S2 is clearly different from the other classes. This is also the case for D. S4 and S5 have quite similar distributions, but these two classes can be discriminated from the other classes. S3, P3Y, P3O, and P4 are also quite similar. By comparing spruce of different ages (the upper half of Figure 5.2) we can see that as the three grows, the relative fraction of shadows within the stand increases. For S2, the distribution is a mixture of several vegetation classes including soil, shrub, deciduous, and conifer. As the three grows, the fraction of underbrush decreases and the shadow fraction increases.

Based on this, we cannot expect to discriminate properly between spruce and pine of the same age given the multispectral image only. We can discriminate properly between the following classes:

- Spruce, cutting class 2
- Spruce and pine, cutting class 3
- Spruce, cutting classes 4 and 5
- Deciduous forest

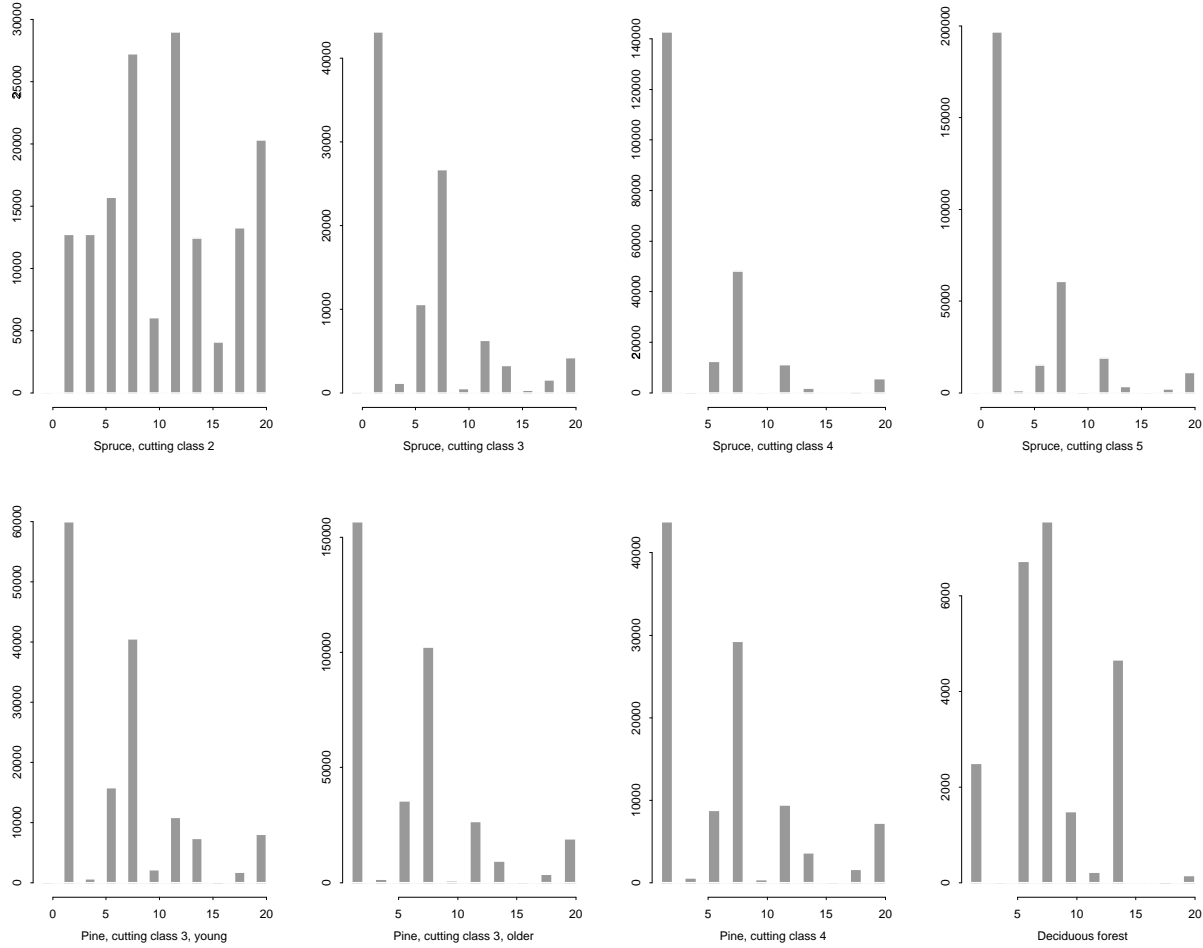


Figure 5.2: *Histograms showing the distribution of the ten spectral classes for the cutting classes S2, S3, S4, S5, P3Y, P3O, P4, D. For each histogram, the x axis shows the spectral classes (which have been assigned the class numbers 2,4,...20), while the y axis shows their frequencies.*

## 5.2 Textural experiments

The main objective of this study has been to determine if parameters like tree type, age and cutting class of a forest stand has influence on typical textural features applied in image processing. So far, the study has been limited to measurements derived from a Gray Level Co-Ocurrence Matrix (GLCM) proposed in (Haralick, Shanmugam & Dinstein 1973).

The test area consists mainly of spruce. Most of the forest stands with pine are mixed with spruce, and there are very few stands containing pine only. Accordingly, the data set is not suitable for a test of distinguishing spruce from pine by texture.

Therefore, we have concentrated on spruce in the experiments. We have selected a set of sub-images from forest stands that are said to contain spruce only. This does not mean that all the trees in the stand (and the sub-image) are spruce. More than 90% of the trees within the stand should be spruce, but there may be single trees or small crops of pine or deciduous trees. The sub-images do not contain deciduous trees, however, no efforts have taken place to exclude pines from the sub-images. The sub-images cover an area of only about  $30 \times 30$  meters. A few pine trees within this area could result in a pine fraction as large as 20-30% (and even higher if one is really unlucky). This could have an influence on the texture. Hopefully, a small number of pines will not change the texture for spruce too much, but this may be a source of error. Because of the lack of pine stands in the data set, we have not performed extensive tests to see how the textural feature values change from spruce to pine.

### 5.2.1 Description of method

The textural features are derived from the so-called Gray Level Co-Ocurrence Matrix (GLCM) (Haralick et al. 1973). The GLCM  $P$  is a  $n \times n$  matrix, where  $n$  is the number of gray levels in the image. A matrix element  $P_d^\theta(i, j)$  is given by the relative frequency of a pixel pair with gray levels  $i$  and  $j$ , respectively, at a distance of  $d$  pixels, and at an angular direction  $\theta$ . Typical values of  $\theta$  are 0, 45, 90 and 135 degrees. We have used the mean value of three directions, horizontal (0 degrees), vertical (-90 degrees) and diagonal (-45 degrees). A GLCM may be calculated for the whole image, “global GLCM”, or in a repetitive manner for a moving window in the image, “local GLCM”. In the first case, the result will be a single textural feature value, and in the second case the result will be a new image where each pixel represents the local texture. (Haralick et al. 1973) have proposed a set of 14 textural features that can be derived from a GLCM. Some other features have been proposed in (Conners, Trivedi & Harlow 1984).

**Global GLCM** In this experiment, we have used a GLCM of dimensionality  $256 \times 256$  and calculated textural measures globally. An efficient method for generation of the  $256 \times 256$  GLCM has been implemented.

**GLCM Spectrum** Earlier attempts to correlate texture to the properties of objects or a phenomenon with spatial repetitive variations have mostly been performed using individual features at a fixed distance. Inspired by the work of (Andrle 1994), and by experiments on sandstone, (Solberg, Andersen, Lyseggen & Koren 1994) and (Koren, Solberg, Halck & Solberg August 1994), our attempt here is to study how textural feature values change as the distance between pairs of pixels is varied. This gives us important information about the change in spatial dependencies within a texture pattern.

## GLCM features

Eight GLCM features were calculated and plotted as functions of the distance between the pixels. These were Inverse Different Moment, Inertia, Absolute Difference Moment, Entropy, Autocorrelation, Covariance, Energy and Uniformity.

### Inverse Difference Moment (IDM)

$$f_{IDM} = \sum_i \sum_j \frac{1}{1 + (i - j)^2} p(i, j) \quad (5.1)$$

IDM is influenced by the homogeneity in the image. A homogeneous scene gives a high IDM value, while an heterogeneous image gives a GLCM with significant values on non-diagonal entries.

### Inertia

$$f_{In} = \sum_i \sum_j (i - j)^2 p(i, j) \quad (5.2)$$

Inertia favours pixel values that deviate much from each other, and, therefore, is a measure of strong variations.

### Absolute Difference Moment (ADM)

$$f_{ADM} = \sum_i \sum_j |i - j| p(i, j) \quad (5.3)$$

The Absolute Difference Moment is related to Inertia and Inverse Difference Moment, all being functions of the difference  $(i - j)$ . The Inverse Difference Moment has good discriminatory capability in the lower contrast range, whereas Inertia is best for high contrasts. The Absolute Difference Moment works equally well for all contrasts without being tailored to a particular contrast range.

## Covariance

$$f_{Cov} = \sum_i \sum_j (i - \mu_x)(j - \mu_y)p(i, j) \quad (5.4)$$

where  $\mu_x$  and  $\mu_y$  are the mean values of  $p_x$  and  $p_y$ . Covariance favours entries that deviate much from the mean value, and, therefore, is a measure of variation.

## Entropy

$$f_{Ent} = -\sum_i \sum_j p(i, j) \log(p(i, j)) \quad (5.5)$$

A complex (heterogeneous) scene will have higher values for Entropy than more simple scenes.

## Autocorrelation

$$f_{AC} = \sum_i \sum_j i j p(i, j) \quad (5.6)$$

The autocorrelation feature is a measure of gray-tone linear dependencies in the image.

## Energy

$$f_{Ener} = \sum_i \sum_j i^2 j^2 p^2(i, j) \quad (5.7)$$

The energy feature is related to the autocorrelation feature. It gives more pronounced differences between images with high and low gray-tone values.

## Uniformity

$$f_U = \sum_i \sum_j p^2(i, j) \quad (5.8)$$

This feature is a measure of uniformity in the image. It will produce large values for uniform images. The value is independent of the mean gray-tone values.

### 5.2.2 GLCM spectra experiments

To see if there is a correspondence between some of the GLCM textural features and the value of age and cutting class, we tested all the described GLCM features. GLCM spectra were derived by varying the pixel-pair distance  $d$ . A “global GLCM” method calculating one feature value for the whole sub-image was applied.

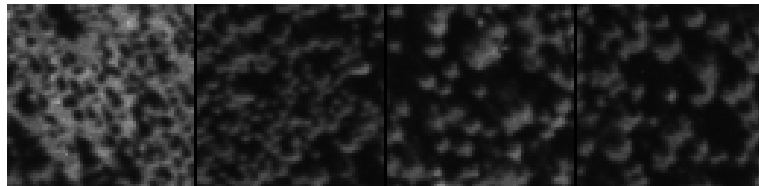


Figure 5.3: *Images of forest stands containing spruce. Site index 14. From left to right, cutting class 2, 3, 4 and 5.*

Forest stand no.	94006-31	94006-40	94005-337	94006-202
Age	15	35	80	110
Cutting class	2	3	4	5

Table 5.1: *Forest stand no., age and cutting class for the stands in the figure above. All stands have 100% spruce.*

In Figures 5.4 to 5.7, we show the spectra of the four textural features which seem to be most useful in forest classification for  $d = 1\text{-}20$  pixels. The spectra have been calculated for four samples of forest stands having site index 14 and belonging to different cutting classes. The samples were located close to nadir to avoid severe imaging effects. The sub-images used are found in Figure 5.3. The forest stand number, age and cutting class for the samples are shown in Table 5.1.

In Figures 5.4 and 5.5, we see that *Uniformity* and *Inverse Difference Moment* seem to discriminate the four cutting classes (5, 4, 3 and 2 from the top) reasonably well, and best for small values of the distance  $d$ . In Figures 5.6 and 5.7, we see that *Autocorrelation* and *Covariance* seem to discriminate well cutting class 2 from the others. These features were then tested on larger sets of data.

### 5.2.3 Forest-parameters-versus-texture experiments

*Uniformity* seems to be one of the GLCM textural features best suited to classify forest stands according to cutting class. In Figure 5.8, the cutting classes of forest stands with 100% spruce has been plotted against *Uniformity* for distance  $d = 1$ . Each stand is marked with its number. There may be more than one image from some of the stands. The data set consists of 84 samples from 53 stands. We see that the mean value of *Uniformity* increases with the cutting class from 2 to 5, but the variation within each class is large, especially for class 5 and 4. The textural feature values overlap for the cutting classes, and it seems to be difficult to determine the correct cutting class directly from the value of *Uniformity*. However, this data set is severely influenced by imaging effects. Many of the sub-images are found at a considerable distance from nadir.

To reduce the imaging effects, the data set was reduced to 34 samples from 21 stands.

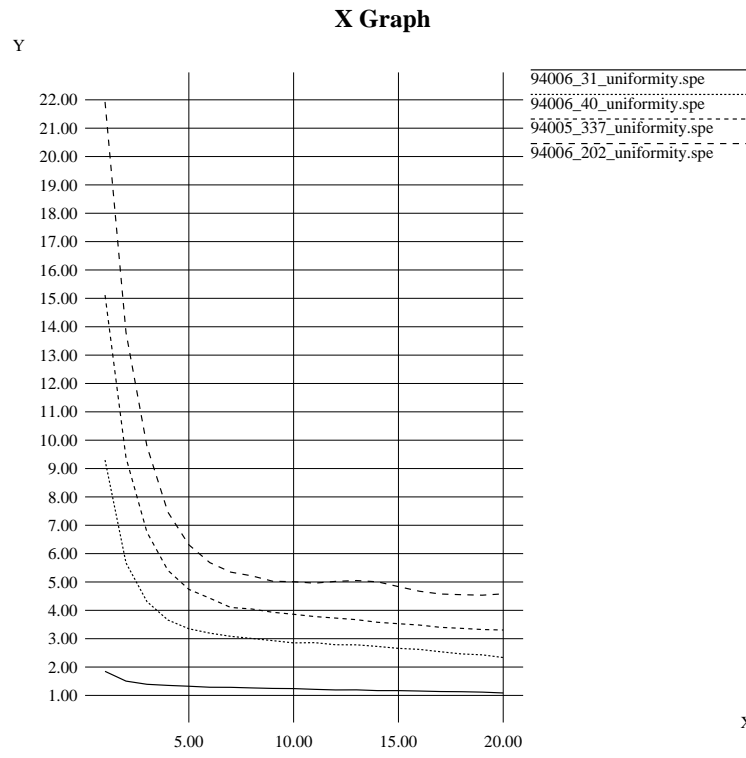


Figure 5.4: Spectra of Uniformity. Cutting class 2, 3, 4 and 5 from the bottom and up.

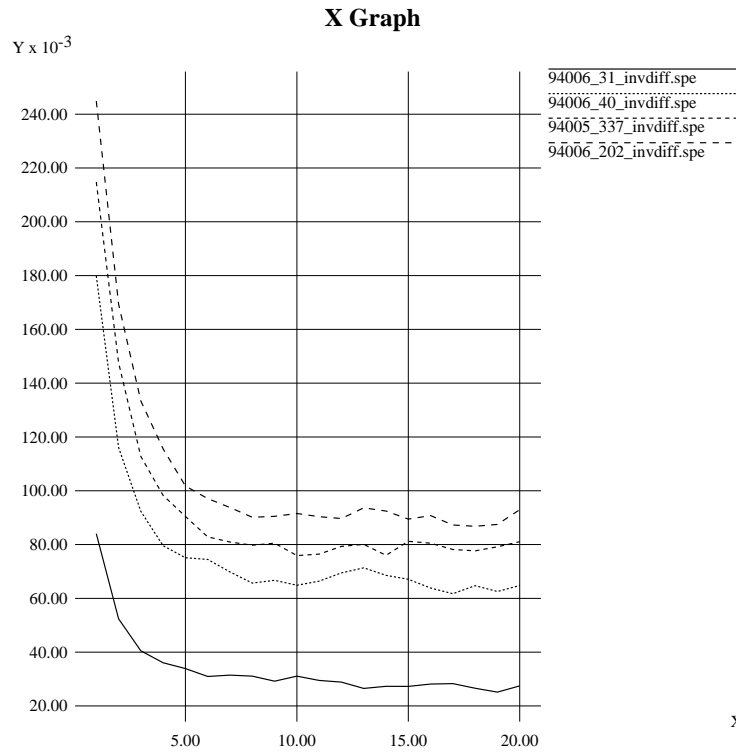


Figure 5.5: Spectra of Inverse Difference Moment. Cutting class 2, 3, 4 and 5 from the bottom and up.

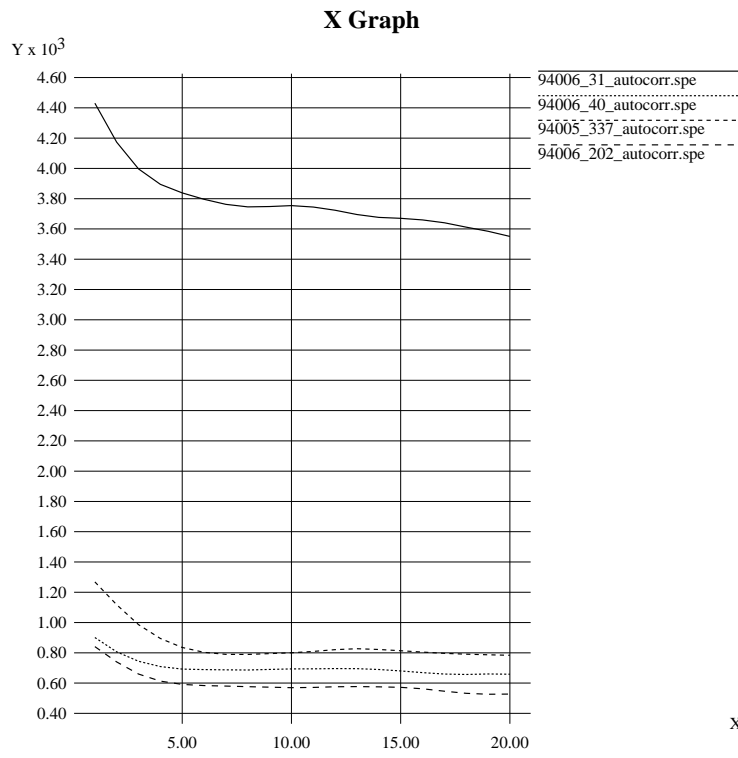


Figure 5.6: *Spectra of Autocorrelation.* Cutting class 2 is well separated from class 3, 4 and 5.

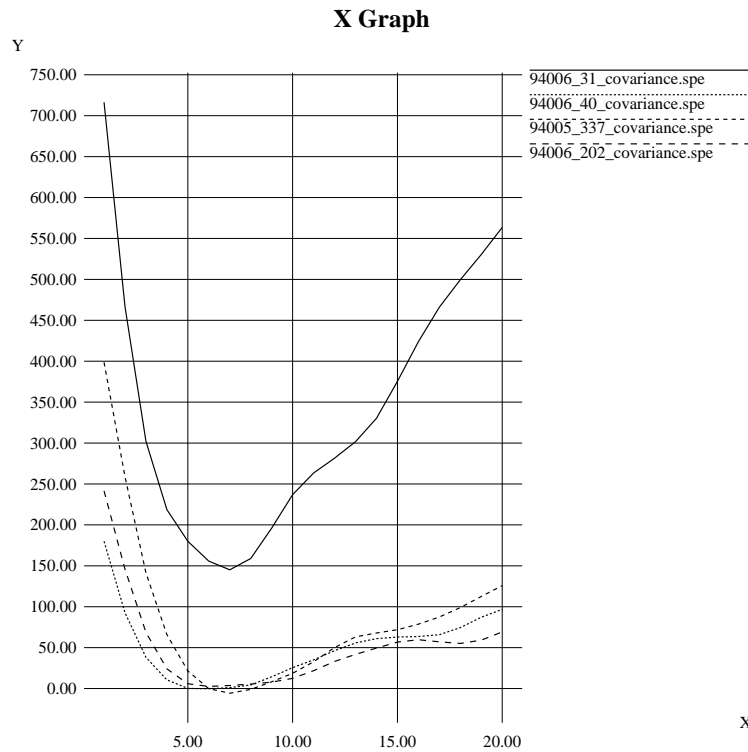


Figure 5.7: *Spectra of Covariance.* Cutting class 2 is well separated from class 3, 4 and 5.

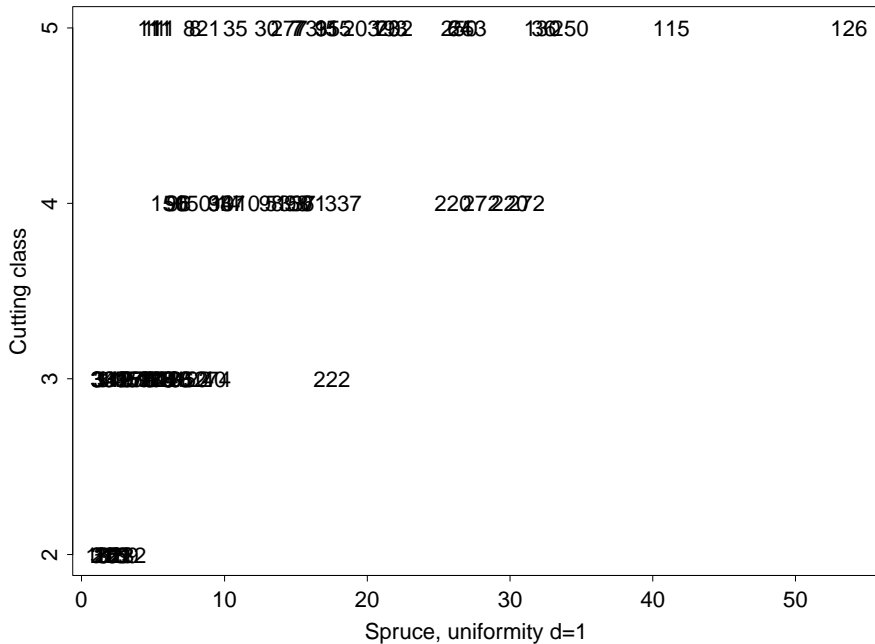


Figure 5.8: Cutting class plotted against Uniformity for 84 samples from 53 forest stands containing spruce only. The numbers correspond to stand numbers.

In Figure 5.9, the same type of plot has been drawn for the new data set. Most of the samples have a centre point closer than 700 meters to nadir. To get a reasonable number of samples of cutting class 4, three samples located between 750 and 800 meters from nadir were included in the set. Cutting class 2 was excluded, because there were few such stands close to nadir.

When reducing the imaging effects, we find smaller variations of the textural feature values within one class, especially for class 5. For each of the classes, there is one stand having a textural value much higher than the others. Forest stand no. 126 is located in a steep hillside to the west of nadir. The hill is falling off to the west and away from the sun, so the shadowing effect increases the value from *Uniformity*. The same topographic effects affect the texture of forest stand 220. It is located to the west of nadir on a slope falling off to northwest. The sub-images may be studied in Figure 2.4.

For cutting class 3, the forest stand no. 222 is quite different from the others. The age of the trees in this stand is 50 years, whereas the other stands of class 3 have ages between 25 and 35. The differences in texture can be studied in Figure 2.4. Here, one can see that the stand no. 222 look more like the ones in cutting class 4.

When removing these 3 stands, we find that the textural feature values are nearly non-overlapping for the three cutting classes.

In Figure 5.10 the same plot is shown for *Inverse Difference Moment*. This plot is quite like the one for *Uniformity*, but there is a greater variation of texture values for cutting

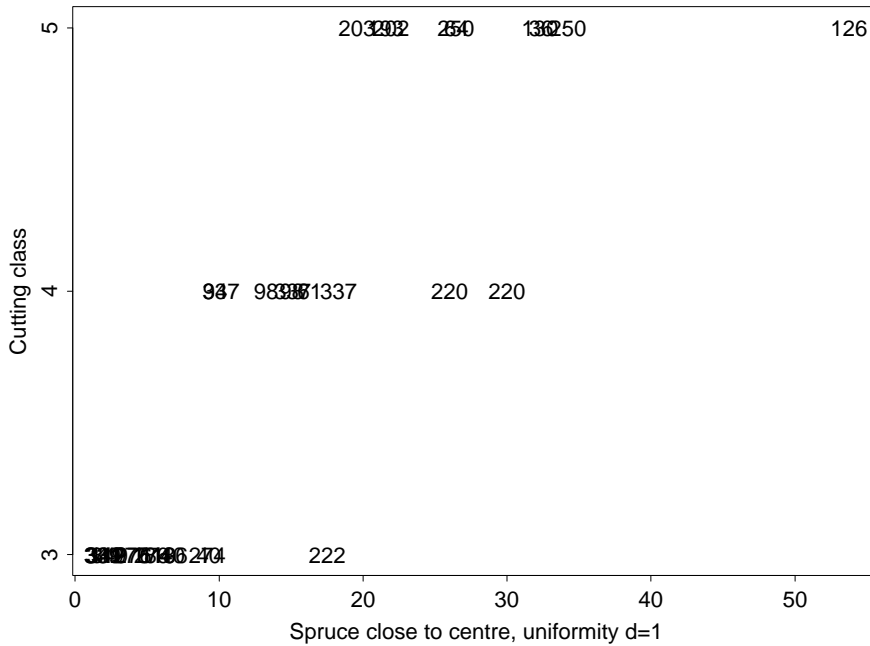


Figure 5.9: *Cutting class as a function of Uniformity for forest stands containing only spruce near nadir.*

class 3.

From Figure 5.8 we see that the value of *Uniformity* does not discriminate cutting classes 2 and 3. This can be done better by other textural features like *Autocorrelation*. Figure 5.11 shows a plot of cutting class as a function of *Autocorrelation* for stands containing only spruce, using the same data set as in Figure 5.8. We see that *Autocorrelation* does not discriminate cutting classes 3, 4 and 5, but the values for cutting class 2 do not overlap much with the others. The data set has not been reduced to remove imaging effects. For cutting class 2 and 1, the imaging effects have less influence, especially for the youngest stands. The trees are small and the ground between the trees are dominating. The effects of shadows are minimal, and both radial distortion and topographic effects may be neglected.

The same conclusions may be drawn from Figure 5.12 where *Covariance* with distance  $d = 20$  has been used.

These few experiments indicate that it may be possible to discriminate forest stands according to cutting classes using texture.

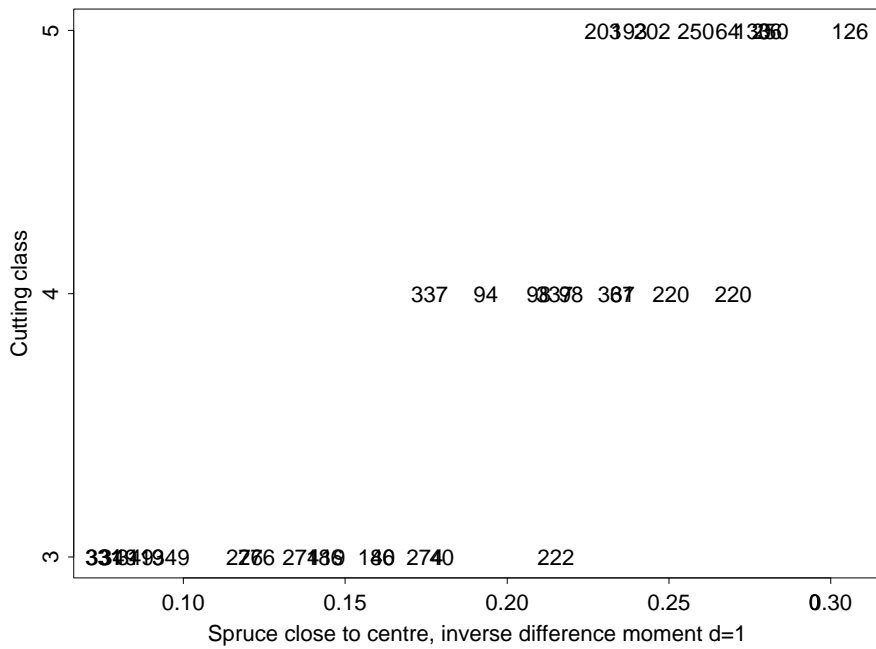


Figure 5.10: *Cutting class as a function of Inverse Difference Moment for forest stands containing only spruce near nadir.*

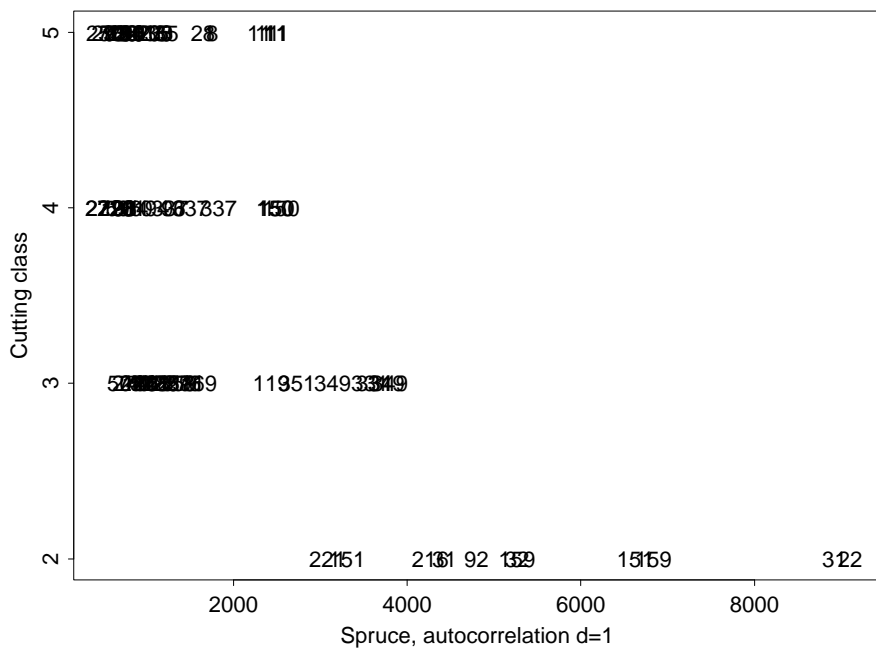


Figure 5.11: *Cutting class as a function of Autocorrelation for forest stands containing only spruce near nadir.*

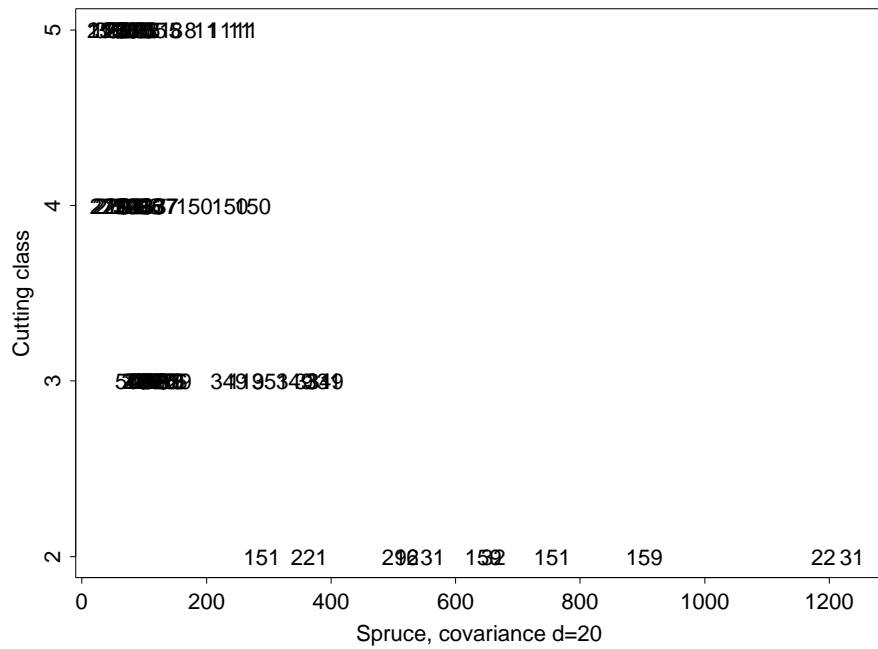


Figure 5.12: *Cutting class as a function of Covariance for forest stands containing only spruce near nadir.*

# Chapter 6

## Discussion and conclusions

The study of imaging effects in aerial photography showed that such effects must be taken into account. Effects due to small errors in the camera's optical system or atmospheric refraction can be neglected here since they are much smaller than the pixel resolution. Radial displacements and distortions must, however, be handled when analyzing data located away from the nadir point. The combined effect of radial distortion of each tree and the solar illumination creates great variations that depend on both the off-nadir distance and the direction relative to the nadir point. These effects are even more exaggerated in non-flat terrain. From the data studied, it seems obviously that the effects must be corrected for practical and robust applications of image analysis in semi-automatic forest mapping. Most of the relevant parameters creating the geometrical effects will be well-known for a given image, so it should be possible to model the effects for correction. The most difficult part of the modelling will probably be the tree modelling, where the result depends on e.g. the tree species.

To relate the spectral information in the three-band image to the desired tree classes and cutting classes, the original image was first segmented into a set of ten natural spectral classes: shadow, soil, shrub, grassland, deciduous forest, non-productive forest land, peat, conifer young and conifer older. The relative distribution of these classes for each cutting class and tree type was examined. As the trees in a stand grow, the fraction of underbrush decreases and the shadow fraction increases. Based on spectral information only, we cannot discriminate properly between spruce and pine of the same age. The following classes can be discriminated: (i) spruce, cutting class 2; (ii) spruce and pine, cutting class 3; (iii) spruce, cutting classes 4 and 5; (iv) deciduous forest.

Experiments with textural measures derived from a Gray Level Co-Ocurrence Matrix show that textural features like *Uniformity* and *Inverse Difference Moment* seem to be useful for discrimination between cutting classes 3, 4 and 5 for stands containing spruce only. However, there will always be problems because there are indistinct limits between the cutting classes. There are no sharp distinctions between the trees at e.g. the upper end of one class and the lower end of the neighbouring class.

To discriminate cutting class 2 (and 1) from the others, textural features like *Autocorrelation* and *Covariance* may be useful. For cutting classes 1 and 2, the image is dominated by the ground between the trees, especially for the younger stands.

Topographic and radial effects have a great influence on the textural feature values. When reducing the data set to contain forest stands located near nadir and removing stands in steep terrain, the experiments gave promising results.

However, the data set used was small and the investigation limited. To be able to make decisive conclusions a much larger set of data must be investigated, and combinations of textural features must be studied.

The focus of the research presented in this report has been the challenge of forest classification based on digitized infrared aerial photos. Interpretation of such demanding imagery has until now exclusively been performed manually. The current research is a first step in the direction of the goal of semi-automatic interpretation of forest imagery. Operational semi-automatic mapping will probably be carried out on data originating from electrooptical and microwave sensors, however, this first steps of research have equally well been carried out on digitized infrared photos. The preliminary results from this initial research presented here is encouraging and support a more thorough work to develop methods adapted particularly for forest analysis and classification.

# Bibliography

- Andrle, R. (1994), ‘The angle measure technique: A new method for characterizing the complexity of geomorphics’, *Journal of Mathematical Geology* pp. 83–97.
- Connors, R., Trivedi, M. & Harlow, C. (1984), ‘Segmentation of a high-resolution urban scene using texture operators’, *Computer Vision, Graphics, and Image Processing* **25**, 273–310.
- Elachi, C. (1987), *Introduction to the Physics and Techniques of Remote Sensing*, John Wiley & Sons.
- Haralick, R., Shanmugam, K. & Dinstein, I. (1973), ‘Textural features for image classification’, *IEEE Transactions on Systems, Man, and Cybernetics SMC-3*, 610–621.
- Herrmann, K., Rock, B., Ammer, U. & Paley, H. (1988), ‘Preliminary assessment of airborne imaging spectrometer and airborne thematic mapper data acquired for forest decline areas in the federal republic of germany’, *Remote Sensing of Environment* **24**, 129–149.
- Howard, J. (1991), *Remote Sensing of Forest Resources - Theory and application*, Chapman & Hall.
- Jain, A. K. & Dubes, R. C. (1988), *Algorithms for Clustering Data*, Prentice Hall, Englewood Cliffs, N. J.
- Koren, H., Solberg, A. S., Halck, O. & Solberg, R. (August 1994), Texture analysis of sandstone surfaces, Technical report, NR Note BILD/08/94, Norwegian Computing Center, Oslo.
- Leckie, D., Yuan, X., Ostaff, D., Piene, H. & MacLean, D. (1992), ‘Analysis of high resolution multispectral meis imagery for spruce budworm damage assessment on a single tree basis’, *Remote Sensing of Environment* **40**, 125–136.
- Nämnden för Skoglig Fjärranalys (1993), *Flygbildsteknik och Fjärranalys*, Nämnden for Skoglig Fjärranalys, Sverige.
- Pilon, P. & Wiart, R. (1990), ‘Operational forest inventory applications using landsat tm data: The british columbia experience’, *Geocarto International* **1**, 25–30.
- Richards, J. (1986), *Remote Sensing Digital Image Analysis, An Introduction*, Springer-Verlag.

Rock, B. (1982), Spatial and spectral resolution necessary for remotely sensed vegetation studies, the multispectral imaging science working group: Final report, vol. 3, Technical report, NASA C.P.-2260.

Rock, B., Hoshizaki, T. & Miller, J. (1988), 'Comparison of in situ and airborne spectral measurements of the blue shift associated with forest decline', *Remote Sensing of Environment* **24** (1), 109–128.

Rock, B., Vogelmann, J., Williams, D., Vogelmann, A. & Hoshizaki, T. (1986), 'Remote detection of forest damage', *BioScience* **36**, 439–445.

Singhroy, V., Stanton-Gray, R. & Springer, J. (Reno, Nevada, Sept. 29 - Oct. 2, 1986), Spectral geobotanical investigation of mineralized till sites, in 'Proceedings of Thematic Conference on Remote Sensing for Exploration of Geology', p. 1986.

Solberg, R. (1985), Geometrical correction of digital imagery in optical satellite remote sensing (in norw.), Technical report, NR Report no. 767, Norwegian Computing Center.

Solberg, R., Andersen, T., Lyseggen, J. & Koren, H. (1994), Prediction of sandstone parameters from texture, Technical report, NR Note BILD/10/94, Norwegian Computing Center, Oslo.

Strand, G.-H. (1989), Remote sensing of forest - an inductive approach, Technical report, Report no. 824, Norwegian Computing Center.

Tapper, G. & Dempsey, D. (Houston, Texas, May 16-19, 1988), Meis ii and surface data intergration for detection of geobotanical anomalies, in 'Proceedings from Thematic Conference on Remote Sensing for Exploration of Geology, Vol. 2'.

Tucker, C. (1976), 'Sensor design for monitoring vegetation canopies', *Photogrammetric Engineering and Remote Sensing* **42**, 1399–1410.